Article

Adaptive Fixed-time Control for Multiple Switched Coupled Neural Networks

Linhao Zhao and Boqian Li*

Australian AI Institute, Faculty of Engineering and Information Technology, University of Technology Sydney, Sydney, NSW 2007, Australia

* Correspondence: BoqianLi@student.uts.edu.au (Boqian Li)

Abstract: Adaptive control is an effective approach for mitigating undesirable deviations in prescribed closed-loop plant behavior. However, conventional adaptive control methods often exhibit slow responses in various control tasks. This paper introduces a novel adaptive control method to achieve fixed-time synchronization in a class of coupled neural networks. We present coupled neural networks with multiple switching topologies and design a fixed-time adaptive control strategy for this system. Furthermore, we establish a criterion to ensure the fixed-time stability of the closed-loop system. Two numerical examples are provided to demonstrate the effectiveness and accuracy of the theoretical results.

Keywords: coupled neural networks with multiple weights; switching topology; fixed-time synchronization; adaptive control

1. Introduction

Coupled neural networks (CNNs) have garnered significant attention due to their applications in secure communication and image encryption [1, 2]. Consequently, extensive research has been conducted on the dynamic behaviors of CNNs [3−5]. Additionally, multi-weighted network models effectively represent real-world networked systems [6, 7], such as social networks, inter-city population flow networks, and urban public traffic networks [8]. leading to considerable study on CNNs with multiple weights and their synchronization [9].

Synchronization, a collective behavior emerging from the dynamic coupling of units, is prevalent in nature, as seen in the blinking of fireflies, the beating of heart cells, and the calling of frogs [10]. Due to its importance, numerous studies have focused on synchronization in CNNs with multiple weights, extending to $\mathcal{H}_\infty$ synchronization, output synchronization, and lag synchronization [11−13]. However, these synchronization methods often operate over infinite timescales, which is impractical for applications like robotic and vehicle platooning control [14, 15]. To address this, finite-time stability was introduced [16] and extended to finite-time synchronization [17−20]. For example, Rao et al. utilized impulsive controllers to achieve average stochastic finite-time synchronization for CNNs with energy-bounded noises [17]. Tang et al. examined finite-time synchronization for CNNs with time-varying delays and Markovian jumping topologies using an intermittent quantized control strategy [18]. Xu et al. studied finite-time synchronization in privacy-preserving complex networks [19]. Tian et al. developed a delay-independent dynamical event-triggered controller for finite-time synchronization in neural-type complex networks with intermittent couplings [20]. Finite-time synchronization has also been extended to multi-weighted network models [21−24]. For instance, Qiu et al. used feedback controllers to address finite-time synchronization in multi-weighted complex networks with and without coupling delays [21]. Xu et al. employed feedback and adaptive controllers for finite-time synchronization in fractional-order complex-valued networks [22]. Zhao et al. addressed finite-time and $\mathcal{H}_\infty$ synchronization in CNNs with multiple state and derivative couplings using nonchattering controllers [23]. Wang et al. discussed finite-time synchronization and $\mathcal{H}_\infty$ synchronization for CNNs with multi-state and multi-derivative couplings [24]. However, the settling time for finite-time synchronization heavily relies on the initial states, limiting its practical application.

To mitigate this limitation, fixed-time stability was proposed [25]. Research has since concentrated on fixed-

time synchronization for both single-weighted [26−28] and multi-weighted network models [29−31]. For example, Chen et al. explored practical fixed-time synchronization of uncertain CNNs using dual-channel event-triggered control methods [26]. Gong et al. investigated finite-time and fixed-time synchronization in coupled memristive neural networks with time delays using appropriate controllers [27]. Guo et al. studied fixed-time synchronization for CNNs with intra-state switching and outer coupled matrix switching using feedback control methods [28]. Cao et al. focused on fixed-time output synchronization in complex networks with multiple state and output couplings using adaptive control strategies [29]. Liu et al. designed economical control strategies for fixed-time synchronization in multi-weighted complex networks [30]. Shi et al. proposed criteria for finite-time and fixed-time synchronization in multi-weighted complex networks using a unified control strategy [31]. Despite these advances, few studies have specifically addressed fixed-time synchronization for multi-weighted networks.

In CNNs, practical factors can lead to switching phenomena in the network topology, such as the addition or removal of links, external interferences in communication channels, and constrained sensing radii within engineering networks [32]. Consequently, researchers have explored synchronization in both single and multi-weighted network models with switching topologies [33−39]. For instance, Hu et al. studied sampled-data-based event-triggered synchronization in fractional and impulsive complex networks with time-varying delays and switching topologies [33]. Yang et al. focused on global exponential cluster synchronization for switched fractional-order complex networks using pinning control strategies [34]. Chen et al. examined synchronization in complex networks with mixed delays and switching topologies [35]. Yang et al. addressed synchronization issues in time-delayed complex networks with switching topologies, considering actuator faults and impulsive effects [37]. Wang et al. explored synchronization in multiple memristive neural networks with switching topologies and parameter mismatches using periodic event-triggered control methods [36]. Additionally, Wang et al. investigated synchronization in multi-weighted complex networks under attack [38]. Cao et al. explored adaptive control methods for synchronization in CNNs with switching topologies [39]. Despite these advancements, few studies have specifically addressed the fixed-time synchronization problem for CNNs with switching topologies.

Inspired by these studies, this paper focuses on adaptive fixed-time synchronization for a class of CNNs with multiple switching topologies. The main contributions are shown as follows:

1. Compared with existing works on fixed-time synchronization [26−31], this paper extends these research results to the case of multiple switching topology.

2. Based on the system model, this paper proposes a novel adaptive fixed-time control strategy and develops a criterion to ensure fixed-time synchronization for a type of CNNs with multiple switching topologies.

The rest of this paper is organized as follows: Section II provides notations and important lemmas. Section III presents the main results. Section IV offers two numerical examples, and Section V concludes the paper.

2. Preliminary

2.1. Notations

$\mathbb{R}$, $\mathbb{R}^{\kappa}$, and $\mathbb{R}^{\kappa \times m}$ denote the set of real numbers, κ-dimensional Euclidean space, and the space of $\kappa \times m$ real matrices, respectively. $\mathbb{K}$ represents the set of natural numbers. $I_{\kappa} \in \mathbb{R}^{\kappa \times \kappa}$ denotes the identity matrix. $\mathcal{G} = (\mathcal{V}, \mathcal{E})$ represents an undirected graph that describes the connectivity interactions among K nodes, where the node set is $\mathcal{V} = \{v_1, v_2, \cdots, v_K\}$ and the edge set is $\mathcal{E} \subset \mathcal{V} \times \mathcal{V}$. We define $sgn^{\phi}(x) = \text{sign}(x)|x|^{\phi}$.

2.2. Lemmas

Lemma 2.1 (Fixed-time Stability [25]). Consider a nonlinear system defined by

$$\dot{v}(\flat) = f(\flat, v(\flat)), \ \flat \in \mathbb{R}+, \ v(0) = v_0, \tag{1}$$

where the state vector $v \in \mathbb{R}^{\kappa}$ and the nonlinear function $f(\flat, x) : \mathbb{R}+ \times \mathbb{R}^{\kappa} \to \mathbb{R}^{\kappa}$. If there exists a continuous and positive definite function $V(x(\flat)) : \mathbb{R}^{\kappa} \to \mathbb{R}$ with radial bounds fulfilling:

1. $V(x(\flat)) = 0 \Leftrightarrow x(\flat) = 0$;

2. Any solution $x(\flat)$ of system (1) satisfies the inequality

$$\dot{V}(x(\flat)) \leqslant - \left(\eta_1 V^{\phi_1}(x(\flat)) + \eta_2 V^{\phi_2}(x(\flat)) \right)^{\alpha}$$

for parameters $\eta_1, \eta_2, \phi_1, \phi_2, \alpha$ with $\phi_1 \alpha > 1$ and $\phi_2 \alpha < 1$,
then the origin of system (1) is said to be fixed-time stable, with the estimated settling time $\tau(x_0)$ satisfying

$$\tau(x_0) \leqslant \tau_{\max} = \frac{1}{\eta_1^{\alpha}(\phi_1 \alpha - 1)} + \frac{1}{\eta_2^{\alpha}(1 - \phi_2 \alpha)}, \quad \forall x_0 \in \mathbb{R}^{\kappa}. \tag{2}$$

Lemma 2.2 (Hölder's Inequality [40]). *For any vector* $x_J \geqslant 0, (J = 1, 2, \cdots, K)$ *and parameters* $\phi_1 > 1, 0 < \phi_2 \leqslant 1$, *then*

$$K^{1-\phi_1}\left(\sum_{J=1}^{K} x_J\right)^{\phi_1} \leqslant \sum_{J=1}^{K} x_J^{\phi_1}, \quad \left(\sum_{J=1}^{K} x_J\right)^{\phi_2} \leqslant \sum_{J=1}^{K} x_J^{\phi_2}. \tag{3}$$

Lemma 2.3 (Kronecker Product [41]). The Kronecker product satisfies the following properties:

$$(Q_1 \otimes Q_2)^T = Q_1^T \otimes Q_2^T, \ (Q_1 \otimes Q_2)^{-1} = Q_1^{-1} \otimes Q_2^{-1},$$
$$(\beta Q_1) \otimes Q_2 = Q_1 \otimes (\beta Q_2), (Q_1 + Q_3) \otimes Q_2 = Q_1 \otimes Q_2 + Q_3 \otimes Q_2$$
$$(Q_1 \otimes Q_2)(Q_3 \otimes Q_4) = (Q_1 Q_3) \otimes (Q_2 Q_4),$$

where β refers to a constant. Q_1, Q_2, Q_3, and Q_4 stand for matrices with suitable dimension.

3. Main Results

3.1. Network Model

Consider a class of multi-weighted CNNs with the switching topology defined by

$$\dot{x}_J(\flat) = -Ax_J(\flat) + Bf(x_J(\flat)) + J + \sum_{m=1}^{M}\sum_{\iota=1}^{K} c_m \alpha_{J\iota}^{m,\rho(\flat)} \Gamma_m x_\iota(\flat) + u_J(\flat), \tag{4}$$

where $J = 1, 2, \cdots, K$ and $m = 1, 2, \cdots, M$ respectively refer to the indices of network nodes and multiple weights associated with coupling. The vector $x_J = (x_{J1}, x_{J2}, \cdots, x_{J\kappa}) \in \mathbb{R}^\kappa$ represents the state of the network. The matrices $A = \text{diag}(a_1, a_2, \cdots, a_\kappa) \in \mathbb{R}^{\kappa \times \kappa}$ and $B = (B_{J\hbar})_{\kappa \times \kappa} \in \mathbb{R}^{\kappa \times \kappa}$ are given. The function $f(x_J(\flat)) = (f_1(x_{J1}(\flat)), f_2(x_{J2}(\flat)), \cdots, f_\kappa(x_{J\kappa}(\flat)))^T \in \mathbb{R}^\kappa$ and the vector $J = (J_1, J_2, \cdots, J_\kappa)^T \in \mathbb{R}^\kappa$ are also defined. The coupling strength is $0 < c_m \in \mathbb{R}$. The matrix $0 < \Gamma_m \in \mathbb{R}^{\kappa \times \kappa}$ indicates the internal coupling matrix. The function $\rho : [0, \infty) \to \Psi = \{1, 2, \cdots, \psi\}$ represents a switching signal, and we define $\rho(\flat)$ can be described as the switching sequence

$$\bar{\rho} = \{(w_0, \flat_0), (w_1, \flat_1), \cdots, (w_k, \flat_k), \cdots \mid w_k \in \Psi, k \in \mathbb{K}\},$$

where w_k corresponds to the sequential number assigned to the activated subsystem at time $\flat_k$. For each $\iota \in \{1, 2, \cdots, \psi\}$, the outer coupling matrix $\alpha^{m,\iota} = (\alpha_{J\hbar})_{K \times K}^{m,\iota} \in \mathbb{R}^{K \times K}$ is defined as follows:

$$\alpha_{J\iota}^{m,\iota} = \begin{cases} \alpha_{\iota J}^{m,\iota} > 0, & \text{if } (J, \iota) \in \mathcal{E}, \\ -\displaystyle\sum_{\substack{p=1 \\ p \neq \iota}}^{K} \alpha_{Jp}^{m,\iota}, & \text{if } J = \iota, \\ 0, & \text{otherwise.} \end{cases}$$

The control input $u_J(\flat) = (u_{J1}(\flat), u_{J2}(\flat), \cdots, u_{J\kappa}(\flat)) \in \mathbb{R}^\kappa$. In this paper, it is necessary for the network (4) to exhibit connectivity, and different coupling forms should possess an identical topology structure. Additionally, we assume that the function $f_\epsilon(\cdot)$ $(\epsilon = 1, 2, \cdots, \kappa)$ satisfies the following inequality:

$$|f_\epsilon(x_1) - f_\epsilon(x_2)| \leqslant \gamma_\epsilon |x_1 - x_2|$$

for any x_1, x_2 and some $0 < \gamma_\epsilon \in \mathbb{R}$.

We define $x^\star(\flat) = \dfrac{1}{K}\displaystyle\sum_{J=1}^{K} x_J(\flat)$, then one has

$$\dot{x}^\star(\flat) = \frac{1}{K}\sum_{J=1}^{K} \dot{x}_J(\flat)$$

$$= -\frac{1}{K}\sum_{J=1}^{K} Ax_J(\flat) + \frac{1}{K}\sum_{J=1}^{K} Bf(x_J(\flat)) + J$$

$$+ \frac{1}{K}\sum_{m=1}^{M}\sum_{\iota=1}^{K} c_m \left(\sum_{J=1}^{K} \alpha_{J\iota}^{m,\iota}\right)\Gamma_m x_\iota(\flat)$$

$$= -Ax^\star(\flat) + \frac{1}{K}\sum_{J=1}^{K} Bf(x_J(\flat)) + J + \frac{1}{K}\sum_{J=1}^{K} u_J(\flat),$$

where vector $x^{\star}(\flat) = (x_1^{\star}(\flat), x_2^{\star}(\flat), \cdots, x_{\kappa}^{\star}(\flat))^T \in \mathbb{R}^{\kappa}$.

The error state is $e_{\jmath}(\flat) = x_{\jmath}(\flat) - x^{\star}(\flat)$ and satisfies

$$\dot{e}_{\jmath}(\flat) = \dot{x}_{\jmath}(\flat) - \dot{x}^{\star}(\flat)$$

$$= -Ax_{\jmath}(\flat) + Ax^{\star}(\flat) + Bf(x_{\jmath}(\flat)) - \frac{1}{K}\sum_{\jmath=1}^{K} Bf(x_{\jmath}(\flat))$$

$$+ \sum_{m=1}^{M}\sum_{\iota=1}^{K} c_m \alpha_{\jmath\iota}^{m,\iota} \Gamma_m x_{\iota}(\flat) + u_{\jmath}(\flat) - \frac{1}{K}\sum_{\jmath=1}^{K} u_{\jmath}(\flat)$$

$$= -Ae_{\jmath}(\flat) + Bf(x_{\jmath}(\flat)) - \frac{1}{K}\sum_{\jmath=1}^{K} Bf(x_{\jmath}(\flat))$$

$$+ \sum_{m=1}^{M}\sum_{\iota=1}^{K} c_m \alpha_{\jmath\iota}^{m,\iota} \Gamma_m (e_{\iota}(\flat) + x^{\star}(\flat)) + u_{\jmath}(\flat) - \frac{1}{K}\sum_{\jmath=1}^{K} u_{\jmath}(\flat)$$

$$= -Ae_{\jmath}(\flat) + Bf(x_{\jmath}(\flat)) - \frac{1}{K}\sum_{\jmath=1}^{K} Bf(x_{\jmath}(\flat))$$

$$+ \sum_{m=1}^{M}\sum_{\iota=1}^{K} c_m \alpha_{\jmath\iota}^{m,\iota} \Gamma_m e_{\iota}(\flat) + u_{\jmath}(\flat) - \frac{1}{K}\sum_{\jmath=1}^{K} u_{\jmath}(\flat),$$

where $e(\flat) = (e_1^T(\flat), e_2^T(\flat), \cdots, e_K^T(\flat))^T \in \mathbb{R}^{K\kappa}$.

Definition 3.1. For any values of $e(0)$, if error state $e(\flat)$ fulfills

$$\lim_{t \to \tau(e(0))} \|e(\flat)\| = 0, \tau(e(0)) \leqslant \tau_{\max}, \tag{5}$$

where $\tau(e(0))$ represents a setting time and $\tau_{\max}$ is a fixed time, then network (4) can achieve fixed-time synchronization.

3.2. Fixed-time Adaptive Control

An adaptive control strategy is designed to ensure that network (4) achieves fixed-time synchronization with the following representation:

$$u_{\jmath}(\flat) = -\sum_{m=1}^{M} c_m k_{\jmath}^m(\flat) \Gamma_m e_{\jmath}(\flat) - \eta_1 sgn^{\phi_1}(e_{\jmath}(\flat)) - \eta_2 sgn^{\phi_2}(e_{\jmath}(\flat)) \tag{6}$$

with the corresponding adaptive law

$$\dot{k}_{\jmath}^m(\flat) = c_m e_{\jmath}^T(\flat) \Gamma_m e_{\jmath}(\flat) - \eta_1 sgn^{\phi_1}\left(k_{\jmath}^m(\flat) - \bar{\varkappa}_{\jmath}^m\right) - \eta_2 sgn^{\phi_2}\left(k_{\jmath}^m(\flat) - \bar{\varkappa}_{\jmath}^m\right), \tag{7}$$

where $\jmath = 1, 2, \cdots, K$. Parameters $\phi_1 > 0, 0 < \phi_2 \leqslant 1, \beta_1 > 0, \beta_2 > 0$, and $\bar{\varkappa}_{\jmath}^m > 0$. The initial value of the adaptive gain $k_{\jmath}^m(0) > 0$.

Remark 3.1. To achieve fixed-time synchronization in a class of CNNs with multiple switching topologies, this paper proposes the adaptive controller (8) and its adaptive law (9). Considering the system model (4) and control objective, the first term is specifically devised in the controller (8) and adaptive law (9). According to the definition of fixed-time stability, we design the second and third terms of the controller (8) and adaptive law (9), enhancing their robustness based on the principles of robust adaptive control methods.

According to (6) and (8), we can get

$$\dot{e}_{\jmath}(\flat) = -Ae_{\jmath}(\flat) + Bf(x_{\jmath}(\flat)) - \frac{1}{K}\sum_{\jmath=1}^{K} Bf(x_{\jmath}(\flat))$$

$$+ \sum_{m=1}^{M}\sum_{\iota=1}^{K} c_m \alpha_{\jmath\iota}^{m,\iota} \Gamma_m e_{\iota}(\flat) - \sum_{m=1}^{M} c_m k_{\jmath}^m(\flat) \Gamma_m e_{\jmath}(\flat)$$

$$- \eta_1 sgn^{\phi_1}(e_{\jmath}(\flat)) - \eta_2 sgn^{\phi_2}(e_{\jmath}(\flat)) - \frac{1}{K}\sum_{\jmath=1}^{K} u_{\jmath}(\flat).$$

Theorem 3.1. If there exist some positive parameters $\varkappa^m = \text{diag}(\bar{\varkappa}_1^m, \bar{\varkappa}_2^m, \cdots, \bar{\varkappa}_K^m)$ such that following inequality holds

$$I_K \otimes (-2A + BB^T + \hat{\gamma}) + 2 \sum_{m=1}^{M} c_m [(\alpha^{m,\iota} - \bar{\varkappa}^m) \otimes \Gamma_m] \leqslant 0,$$

then network (4) is fixed-time synchronization by using controller (8) and the settling time function is globally bounded by $\tau_{\max}$ defined by

$$\tau_{\max} := \frac{1}{\tilde{\eta}_1(\phi_1 - 1)} + \frac{1}{\eta_2(1 - \phi_2)},$$

where $\tilde{\eta}_1 = \min \left\{ 2^{\frac{3-\phi_1}{2}} \eta_1 (MK)^{\frac{1-\phi_1}{2}}, 2^{\frac{3-\phi_1}{2}} \eta_1 (\kappa K)^{\frac{1-\phi_1}{2}} \right\}.$

Proof. Construct the following Lyapunov function for network (4)

$$V(\mathfrak{b}) = \sum_{\mathcal{J}=1}^{K} e_{\mathcal{J}}^T(\mathfrak{b}) e_{\mathcal{J}}(\mathfrak{b}) + \sum_{m=1}^{M} \sum_{\mathcal{J}=1}^{K} \left(k_{\mathcal{J}}^m(\mathfrak{b}) - \bar{\varkappa}_{\mathcal{J}}^m \right)^2.$$

Based on (13), one derives

$$\dot{V}(\mathfrak{b}) = 2 \sum_{\mathcal{J}=1}^{K} e_{\mathcal{J}}^T(\mathfrak{b}) \dot{e}_{\mathcal{J}}(\mathfrak{b}) + 2 \sum_{m=1}^{M} \sum_{\mathcal{J}=1}^{K} \left(k_{\mathcal{J}}^m(\mathfrak{b}) - \bar{\varkappa}_{\mathcal{J}}^m \right) \dot{k}_{\mathcal{J}}^m(\mathfrak{b})$$

$$= 2 \sum_{\mathcal{J}=1}^{K} e_{\mathcal{J}}^T(\mathfrak{b}) \left(-A e_{\mathcal{J}}(\mathfrak{b}) + B f(x_{\mathcal{J}}(\mathfrak{b})) - \frac{1}{K} \sum_{\mathcal{J}=1}^{K} B f(x_{\mathcal{J}}(\mathfrak{b})) \right.$$

$$+ \sum_{m=1}^{M} \sum_{\iota=1}^{K} c_m \alpha_{\mathcal{J}\iota}^{m,\iota} \Gamma_m e_{\iota}(\mathfrak{b}) - \sum_{m=1}^{M} c_m k_{\mathcal{J}}^m(\mathfrak{b}) \Gamma_m e_{\mathcal{J}}(\mathfrak{b})$$

$$\left. -\eta_1 sgn^{\phi_1}(e_{\mathcal{J}}(\mathfrak{b})) - \eta_2 sgn^{\phi_2}(e_{\mathcal{J}}(\mathfrak{b})) - \frac{1}{K} \sum_{\mathcal{J}=1}^{K} u_{\mathcal{J}}(\mathfrak{b}) \right)$$

$$- 2\eta_1 \sum_{m=1}^{M} \sum_{\mathcal{J}=1}^{K} \left| k_{\mathcal{J}}^m(\mathfrak{b}) - \bar{\varkappa}_{\mathcal{J}}^m \right|^{\phi_1+1} - 2\eta_2 \sum_{m=1}^{M} \sum_{\mathcal{J}=1}^{K} \left| k_{\mathcal{J}}^m(\mathfrak{b}) - \bar{\varkappa}_{\mathcal{J}}^m \right|^{\phi_2+1}$$

$$+ 2 \sum_{m=1}^{M} \sum_{\mathcal{J}=1}^{K} c_m \left(k_{\mathcal{J}}^m(\mathfrak{b}) - \bar{\varkappa}_{\mathcal{J}}^m \right) e_{\mathcal{J}}^T(\mathfrak{b}) \Gamma_m e_{\mathcal{J}}(\mathfrak{b})$$

$$= 2 \sum_{\mathcal{J}=1}^{K} e_{\mathcal{J}}^T(\mathfrak{b}) \left(-A e_{\mathcal{J}}(\mathfrak{b}) + B f(x_{\mathcal{J}}(\mathfrak{b})) - B f(x^\star(\mathfrak{b})) + B f(x^\star(\mathfrak{b})) \right.$$

$$- \frac{1}{K} \sum_{\mathcal{J}=1}^{K} B f(x_{\mathcal{J}}(\mathfrak{b})) + \sum_{m=1}^{M} \sum_{\iota=1}^{K} c_m \alpha_{\mathcal{J}\iota}^{m,\iota} \Gamma_m e_{\iota}(\mathfrak{b}) - \sum_{m=1}^{M} c_m k_{\mathcal{J}}^m(\mathfrak{b}) \Gamma_m e_{\mathcal{J}}(\mathfrak{b})$$

$$\left. -\eta_1 sgn^{\phi_1}(e_{\mathcal{J}}(\mathfrak{b})) - \eta_2 sgn^{\phi_2}(e_{\mathcal{J}}(\mathfrak{b})) - \frac{1}{K} \sum_{\mathcal{J}=1}^{K} u_{\mathcal{J}}(\mathfrak{b}) \right)$$

$$- 2\eta_1 \sum_{m=1}^{M} \sum_{\mathcal{J}=1}^{K} \left| k_{\mathcal{J}}^m(\mathfrak{b}) - \bar{\varkappa}_{\mathcal{J}}^m \right|^{\phi_1+1} - 2\eta_2 \sum_{m=1}^{M} \sum_{\mathcal{J}=1}^{K} \left| k_{\mathcal{J}}^m(\mathfrak{b}) - \bar{\varkappa}_{\mathcal{J}}^m \right|^{\phi_2+1}$$

$$+ 2 \sum_{m=1}^{M} \sum_{\mathcal{J}=1}^{K} c_m \left(k_{\mathcal{J}}^m(\mathfrak{b}) - \bar{\varkappa}_{\mathcal{J}}^m \right) e_{\mathcal{J}}^T(\mathfrak{b}) \Gamma_m e_{\mathcal{J}}(\mathfrak{b}).$$

According to the assumption of function $f(\cdot)$, we can obtain

$$2 \sum_{\mathcal{J}=1}^{K} e_{\mathcal{J}}^T(\mathfrak{b}) B(f(x_{\mathcal{J}}(\mathfrak{b})) - f(x^\star(\mathfrak{b}))) \leqslant \sum_{\mathcal{J}=1}^{K} e_{\mathcal{J}}^T(\mathfrak{b}) \left(BB^T + \hat{\gamma} \right) e_{\mathcal{J}}(\mathfrak{b}),$$

where $\hat{\gamma} = \mathrm{diag}(\gamma_1^2, \gamma_2^2, \cdots, \gamma_\kappa^2) \in \mathbb{R}^{\kappa \times \kappa}$.

Then, one has

$$\sum_{\jmath=1}^{K} e_{\jmath}(\mathrm{b}) = \sum_{\jmath=1}^{K} (x_{\jmath}(\mathrm{b}) - x^{\star}(\mathrm{b}))$$

$$= \sum_{\jmath=1}^{K} \left(x_{\jmath}(\mathrm{b}) - \frac{1}{K} \sum_{\jmath=1}^{K} x_{\jmath}(\mathrm{b}) \right)$$

$$= \sum_{\jmath=1}^{K} x_{\jmath}(\mathrm{b}) - \sum_{\jmath=1}^{K} x_{\jmath}(\mathrm{b})$$

$$= 0.$$

From (16), we can derive

$$\sum_{\jmath=1}^{K} e_{\jmath}^{T}(\mathrm{b}) \left(Bf(x^{\star}(\mathrm{b})) - \frac{1}{K} \sum_{\jmath=1}^{K} Bf(x_{\jmath}(\mathrm{b})) - \frac{1}{K} \sum_{\jmath=1}^{K} u_{\jmath}(\mathrm{b}) \right) = 0.$$

With the help of (3), one has

$$\sum_{\jmath=1}^{K} e_{\jmath}^{T}(\mathrm{b}) sgn^{\phi_1}(e_{\jmath}(\mathrm{b})) = \sum_{\jmath=1}^{K} e_{\jmath}^{T}(\mathrm{b})\mathrm{sign}(e_{\jmath}(\mathrm{b}))|e_{\jmath}(\mathrm{b})|^{\phi_1}$$

$$= \sum_{\jmath=1}^{K} \sum_{r=1}^{\kappa} |e_{\jmath r}(\mathrm{b})|^{\phi_1+1}$$

$$= \sum_{\jmath=1}^{K} \sum_{r=1}^{\kappa} (e_{\jmath r}^{2}(\mathrm{b}))^{\frac{\phi_1+1}{2}}$$

$$\geqslant (\kappa K)^{\frac{1-\phi_1}{2}} \left(\sum_{\jmath=1}^{K} e_{\jmath}^{T}(\mathrm{b}) e_{\jmath}(\mathrm{b}) \right)^{\frac{\phi_1+1}{2}},$$

$$\sum_{m=1}^{M} \sum_{\jmath=1}^{K} \left| k_{\jmath}^{m}(\mathrm{b}) - \bar{\varkappa}_{\jmath}^{m} \right|^{\phi_1+1} = \sum_{m=1}^{M} \sum_{\jmath=1}^{K} \left[(k_{\jmath}^{m}(\mathrm{b}) - \bar{\varkappa}_{\jmath}^{m})^{2} \right]^{\frac{\phi_1+1}{2}}$$

$$\geqslant (MK)^{\frac{1-\phi_1}{2}} \left[\sum_{m=1}^{M} \sum_{\jmath=1}^{K} (k_{\jmath}^{m}(\mathrm{b}) - \bar{\varkappa}_{\jmath}^{m})^{2} \right]^{\frac{\phi_1+1}{2}},$$

$$\sum_{\jmath=1}^{K} e_{\jmath}^{T}(\mathrm{b}) sgn^{\phi_2}(e_{\jmath}(\mathrm{b})) = \sum_{\jmath=1}^{K} e_{\jmath}^{T}(\mathrm{b})\mathrm{sign}(e_{\jmath}(\mathrm{b}))|e_{\jmath}(\mathrm{b})|^{\phi_2}$$

$$= \sum_{\jmath=1}^{K} \sum_{r=1}^{\kappa} |e_{\jmath r}(\mathrm{b})|^{\phi_2+1}$$

$$= \sum_{\jmath=1}^{K} \sum_{r=1}^{\kappa} (e_{\jmath r}^{2}(\mathrm{b}))^{\frac{\phi_2+1}{2}}$$

$$\geqslant \left(\sum_{\jmath=1}^{N} e_{\jmath}^{T}(\mathrm{b}) e_{\jmath}(\mathrm{b}) \right)^{\frac{\phi_2+1}{2}},$$

$$\sum_{m=1}^{M} \sum_{\jmath=1}^{K} \left| k_{\jmath}^{m}(\mathrm{b}) - \bar{\varkappa}_{\jmath}^{m} \right|^{\phi_2+1} = \sum_{m=1}^{M} \sum_{\jmath=1}^{K} \left[(k_{\jmath}^{m}(\mathrm{b}) - \bar{\varkappa}_{\jmath}^{m})^{2} \right]^{\frac{\phi_2+1}{2}}$$

$$\geqslant \left[\sum_{m=1}^{M} \sum_{\jmath=1}^{K} (k_{\jmath}^{m}(\mathrm{b}) - \bar{\varkappa}_{\jmath}^{m})^{2} \right]^{\frac{\phi_2+1}{2}}.$$

Substituting (15), (16), and (18) into (14), we can get

$$\dot{V}(\mathfrak{b}) \leqslant \sum_{\mathcal{J}=1}^{K} e_{\mathcal{J}}^{T}(\mathfrak{b}) \left(-2A + BB^{T} + \hat{\gamma} - 2 \sum_{m=1}^{M} c_{m} \bar{\varkappa}_{\mathcal{J}}^{m} \Gamma_{m} \right) e_{\mathcal{J}}(\mathfrak{b})$$

$$+ \sum_{m=1}^{M} \sum_{\mathcal{J}=1}^{K} \sum_{\iota=1}^{K} 2 c_{m} \alpha_{\mathcal{J}\iota}^{m,\iota} e_{\mathcal{J}}^{T}(\mathfrak{b}) \Gamma_{m} e_{\iota}(\mathfrak{b}) - 2\eta_{2} \left(\sum_{\mathcal{J}=1}^{K} e_{\mathcal{J}}^{T}(\mathfrak{b}) e_{\mathcal{J}}(\mathfrak{b}) \right)^{\frac{\phi_{2}+1}{2}}$$

$$- 2\eta_{1}(\kappa K)^{\frac{1-\phi_{1}}{2}} \left(\sum_{\mathcal{J}=1}^{K} e_{\mathcal{J}}^{T}(\mathfrak{b}) e_{\mathcal{J}}(\mathfrak{b}) \right)^{\frac{\phi_{1}+1}{2}} - 2\eta_{2} \left[\sum_{m=1}^{M} \sum_{\mathcal{J}=1}^{K} (k_{\mathcal{J}}^{m}(\mathfrak{b}) - \bar{\varkappa}_{\mathcal{J}}^{m})^{2} \right]^{\frac{\phi_{2}+1}{2}}$$

$$- 2\eta_{1}(MK)^{\frac{1-\phi_{1}}{2}} \left[\sum_{m=1}^{M} \sum_{\mathcal{J}=1}^{K} (k_{\mathcal{J}}^{m}(\mathfrak{b}) - \bar{\varkappa}_{\mathcal{J}}^{m})^{2} \right]^{\frac{\phi_{1}+1}{2}}$$

$$= e^{T}(\mathfrak{b}) \left\{ I_{K} \otimes (-2A + BB^{T} + \hat{\gamma}) + 2 \sum_{m=1}^{M} c_{m} \left[(\alpha^{m,\iota} - \varkappa^{m}) \otimes \Gamma_{m} \right] \right\} e(\mathfrak{b})$$

$$- 2\eta_{2} V^{\frac{\phi_{2}+1}{2}}(\mathfrak{b}) - 2\eta_{1}(\kappa K)^{\frac{1-\phi_{1}}{2}} \left(\sum_{\mathcal{J}=1}^{K} e_{\mathcal{J}}^{T}(\mathfrak{b}) e_{\mathcal{J}}(\mathfrak{b}) \right)^{\frac{\phi_{1}+1}{2}}$$

$$- 2\eta_{1}(MK)^{\frac{1-\phi_{1}}{2}} \left[\sum_{m=1}^{M} \sum_{\mathcal{J}=1}^{K} (k_{\mathcal{J}}^{m}(\mathfrak{b}) - \bar{\varkappa}_{\mathcal{J}}^{m})^{2} \right]^{\frac{\phi_{1}+1}{2}}.$$

According to Theorem 3.1 and (3), one obtains from (19) that

$$\dot{V}(\mathfrak{b}) \leqslant - 2\eta_{2} V^{\frac{\phi_{2}+1}{2}}(\mathfrak{b}) - 2\eta_{1}(\kappa K)^{\frac{1-\phi_{1}}{2}} \left(\sum_{\mathcal{J}=1}^{K} e_{\mathcal{J}}^{T}(\mathfrak{b}) e_{\mathcal{J}}(\mathfrak{b}) \right)^{\frac{\phi_{1}+1}{2}}$$

$$- 2\eta_{1}(MK)^{\frac{1-\phi_{1}}{2}} \left[\sum_{m=1}^{M} \sum_{\mathcal{J}=1}^{K} (k_{\mathcal{J}}^{m}(\mathfrak{b}) - \bar{\varkappa}_{\mathcal{J}}^{m})^{2} \right]^{\frac{\phi_{1}+1}{2}}$$

$$\leqslant - 2\eta_{2} V^{\frac{\phi_{2}+1}{2}}(\mathfrak{b}) - 2\tilde{\eta}_{1} V^{\frac{\phi_{1}+1}{2}}(\mathfrak{b}).$$

Consequently, we conclude that $V(\mathfrak{b}) = 0, t \geqslant \tau_{\max}$ and the estimated settling time can be derived as

$$\tau(e(0)) \leqslant \tau_{\max} = \frac{1}{\tilde{\eta}_{1}(\phi_{1} - 1)} + \frac{1}{\eta_{2}(1 - \phi_{2})}.$$

Then, one can prove that $\lim_{t \to \tau(e(0))} \|e(\mathfrak{b})\| = 0, \|e(\mathfrak{b})\| = 0, t \geqslant \tau_{\max}$.

Remark 3.2. This paper designs a novel adaptive controller (8) to assist system (4) in achieving fxied-time synchronization. Note that the proposed adaptive controller (8) can be applied in other nonlinear systems, such as vehicle platooning system [15] and memristive neural networks system [37].

Remark 3.3. This main difficulty in dealing with fixed-time synchronization for CNNs with multiple switching topologies by using the adaptive fixed-time control method comes from the switching topology, multiple weights and design of adaptive fixed-time control strategy.

4. Numerical Examples

To illustrate the theoretical results and the effectiveness of the designed fixed-time adaptive control strategy, this section provides three numerical examples.

Example 4.1. This example considers a class of CNNs with multiple switching topologies, where the network consists of five nodes with three dimensions each. Furthermore, we select a commonly used activation function [11]:

$$\dot{x}_{\mathcal{J}}(\mathfrak{b}) = - A x_{\mathcal{J}}(\mathfrak{b}) + B f(x_{\mathcal{J}}(\mathfrak{b})) + J + 0.3 \sum_{\iota=1}^{5} \alpha_{\mathcal{J}\iota}^{1,\iota} \Gamma_{1} x_{\iota}(\mathfrak{b})$$

$$+ 0.5 \sum_{\iota=1}^{5} \alpha_{\mathcal{J}\iota}^{2,\iota} \Gamma_{2} x_{\iota}(\mathfrak{b}) + u_{\mathcal{J}}(\mathfrak{b}),$$

where $\mathcal{J} = 1, 2, \cdots, 5, \iota = 1, 2. A = \mathrm{diag}(0.7, 0.5, 0.8), J = (0.3, 0.5, 0.4)^{T}. \Gamma_{1} = \mathrm{diag}(0.8, 0.8, 0.9), \Gamma_{2} = \mathrm{diag}(0.4, 0.5, 0.7). f_{\epsilon}(x) = 0.25(|x+1| - |x-1|), \epsilon = 1, 2, 3.$ The matrices are chosen as

$$B = \begin{pmatrix} 0.2 & 0.2 & 0.2 \\ 0.1 & 0.1 & 0.2 \\ 0.3 & 0.1 & 0.2 \end{pmatrix}. \tag{8}$$

Then, there are four probably topologies $\alpha^{1,1}, \alpha^{1,2}, \alpha^{2,1}$, and $\alpha^{2,2}$, and could be defined by $\alpha^{1,1} \to \alpha^{1,2} \to \alpha^{1,1} \to \cdots$ and $\alpha^{2,1} \to \alpha^{2,2} \to \alpha^{2,1} \to \cdots$. The corresponding outer matrices are

$$\alpha^{1,1} = \begin{pmatrix} -0.5 & 0.3 & 0 & 0.2 & 0 \\ 0.3 & -0.6 & 0.3 & 0 & 0 \\ 0 & 0.3 & -0.4 & 0 & 0.1 \\ 0.2 & 0 & 0 & -0.3 & 0.1 \\ 0 & 0 & 0.1 & 0.1 & -0.2 \end{pmatrix},$$

$$\alpha^{1,2} = \begin{pmatrix} -0.6 & 0.4 & 0 & 0 & 0.2 \\ 0.4 & -0.7 & 0 & 0.3 & 0 \\ 0 & 0 & -0.2 & 0.2 & 0 \\ 0 & 0.3 & 0.2 & -0.5 & 0 \\ 0.2 & 0 & 0 & 0 & -0.2 \end{pmatrix},$$

$$\alpha^{2,1} = \begin{pmatrix} -0.8 & 0.4 & 0 & 0.4 & 0 \\ 0.4 & -0.5 & 0.1 & 0 & 0 \\ 0 & 0.1 & -0.3 & 0 & 0.2 \\ 0.4 & 0 & 0 & -0.7 & 0.3 \\ 0 & 0 & 0.2 & 0.3 & -0.5 \end{pmatrix},$$

$$\alpha^{2,2} = \begin{pmatrix} -0.7 & 0.3 & 0 & 0 & 0.4 \\ 0.3 & -0.4 & 0 & 0.1 & 0 \\ 0 & 0 & -0.2 & 0.2 & 0 \\ 0 & 0.1 & 0.2 & -0.3 & 0 \\ 0.4 & 0 & 0 & 0 & -0.4 \end{pmatrix}.$$

According to the definition of $f_\epsilon(\cdot)(\epsilon = 1, 2, 3)$, we can obtain $\gamma_\epsilon = 0.5$. By exploiting the YALMIP toolbox, we can obtain the following matrices:

Under $\alpha^{1,1}$ and $\alpha^{2,1}$

$$\varkappa^1 = \text{diag}(3.9739, 4.0064, 4.0740, 4.0202, 4.0728),$$
$$\varkappa^2 = \text{diag}(3.7957, 3.8304, 3.8989, 3.8420, 3.8956).$$

Under $\alpha^{1,2}$ and $\alpha^{2,2}$

$$\varkappa^1 = \text{diag}(3.6922, 3.7243, 3.8537, 3.7737, 3.8159),$$
$$\varkappa^2 = \text{diag}(3.5265, 3.5609, 3.6904, 3.6106, 3.6512).$$

We select the parameters $\eta_1 = 2$, $\eta_2 = 3$, $\phi_1 = 2$, and $\phi_2 = 0.6$. The fixed time is calculated as $\tau_{max} = 11.4399$ seconds. The simulation results are displayed in Figures 1 and 2. Figure 1 shows that the values of $\|e_{\mathcal{J}}(\flat)\|$ decrease to zero before the fixed time τ_{max}. As depicted in Figure 2, the values of $k_{\mathcal{J}}^m(\flat)$ converge to positive bounded values. Consequently, the network (22) achieves fixed-time synchronization, as validated by Theorem 3.1 and controller (8).
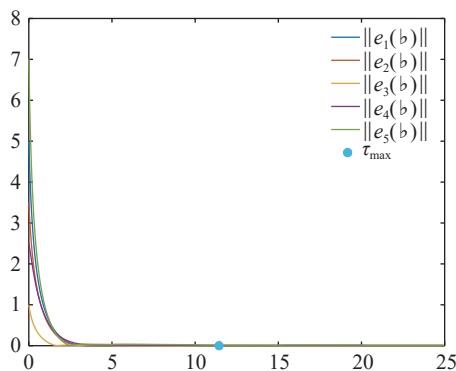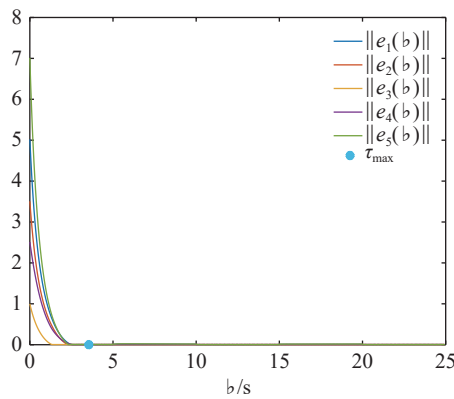

Figure 1. Evolution of $\|e_{\mathcal{J}}(\flat)\|$, $\mathcal{J} = 1, 2, \cdots, 5$ for system (22) via controller (8) with settling time $\tau_{max} = 11.4399$ s.
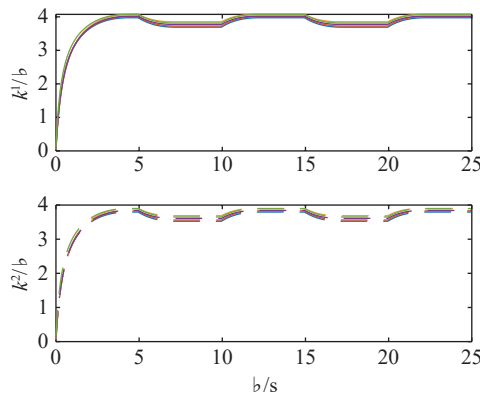
Figure 2. Evolution of adaptive gains $k_j^m(\flat), m = 1, 2$ of controller (8).

Example 4.2. This example studies a class of CNNs with multiple switching topologies, where the network is composed of five nodes, each with three dimensions. Moreover, we select $tan(\cdot)$ as the activation function [13]:

$$\dot{x}_{\jmath}(\flat) = -Ax_{\jmath}(\flat) + Bf(x_{\jmath}(\flat)) + J + 0.4\sum_{\iota=1}^{5}\alpha_{\jmath\iota}^{1,\iota}\Gamma_1 x_{\iota}(\flat)$$

$$+ 0.6\sum_{\iota=1}^{5}\alpha_{\jmath\iota}^{2,\iota}\Gamma_2 x_{\iota}(\flat) + u_{\jmath}(\flat),$$

where $\jmath = 1, 2, \cdots, 5, \iota = 1, 2$. $A = \text{diag}(0.3, 0.6, 0.2), J = (0,0,0)^T . \Gamma_1 = \text{diag}(0.3, 0.4, 0.3), \Gamma_2 = \text{diag}(0.2, 0.3, 0.4)$. $f_\epsilon(x) = \tanh(x), \epsilon = 1, 2, 3$. The matrices are chosen as

$$B = \begin{pmatrix} 0.4 & 0.1 & 0.3 \\ 0.2 & 0.3 & 0.3 \\ 0.1 & 0.2 & 0.5 \end{pmatrix}. \tag{9}$$

Then, there are four probably topologies $\alpha^{1,1}, \alpha^{1,2}, \alpha^{2,1}$, and $\alpha^{2,2}$, and could be defined by $\alpha^{1,1} \to \alpha^{1,2} \to \alpha^{1,1} \to \cdots$ and $\alpha^{2,1} \to \alpha^{2,2} \to \alpha^{2,1} \to \cdots$. The corresponding outer matrices are

$$\alpha^{1,1} = \begin{pmatrix} -0.3 & 0.1 & 0 & 0.2 & 0 \\ 0.1 & -0.2 & 0.1 & 0 & 0 \\ 0 & 0.1 & -0.2 & 0 & 0.1 \\ 0.2 & 0 & 0 & -0.3 & 0.1 \\ 0 & 0 & 0.1 & 0.1 & -0.2 \end{pmatrix},$$

$$\alpha^{1,2} = \begin{pmatrix} -0.3 & 0.1 & 0 & 0 & 0.2 \\ 0.1 & -0.5 & 0 & 0.4 & 0 \\ 0 & 0 & -0.3 & 0.3 & 0 \\ 0 & 0.4 & 0.3 & -0.7 & 0 \\ 0.2 & 0 & 0 & 0 & -0.2 \end{pmatrix},$$

$$\alpha^{2,1} = \begin{pmatrix} -1.8 & 1.4 & 0 & 0.4 & 0 \\ 1.4 & -2.5 & 1.1 & 0 & 0 \\ 0 & 1.1 & -1.4 & 0 & 0.3 \\ 0.4 & 0 & 0 & -0.9 & 0.5 \\ 0 & 0 & 0.3 & 0.5 & -0.8 \end{pmatrix},$$

$$\alpha^{2,2} = \begin{pmatrix} -1.7 & 0.3 & 0 & 0 & 1.4 \\ 0.3 & -0.9 & 0 & 0.6 & 0 \\ 0 & 0 & -0.5 & 0.5 & 0 \\ 0 & 0.6 & 0.5 & -1.1 & 0 \\ 1.4 & 0 & 0 & 0 & -1.4 \end{pmatrix}.$$

According to the definition of $f_\epsilon(\cdot)(\epsilon = 1, 2, 3)$, we can obtain $\gamma_\epsilon = 1$. By using the YALMIP toolbox, one obtains the following matrices:

Under $\alpha^{1,1}$ and $\alpha^{2,1}$

$$\varkappa^1 = \text{diag}(5.8466, 5.7193, 5.9503, 6.0387, 6.0863),$$
$$\varkappa^2 = \text{diag}(6.0396, 5.8595, 6.1790, 6.3101, 6.3729).$$

Under $\alpha^{1,2}$ and $\alpha^{2,2}$

$$\varkappa^1 = \text{diag}(6.0080, 6.1265, 6.2717, 6.0396, 6.1064),$$
$$\varkappa^2 = \text{diag}(6.2220, 6.3973, 6.5996, 6.2831, 6.3571).$$

We choose parameters $\eta_1 = 3$, $\eta_2 = 3$, $\phi_1 = 1.5$, and $\phi_2 = 0.3$. The fixed time is calculated as $\tau_{max} = 3.54671$ seconds. The simulation results are displayed in Figures 3 and 4. In Figure 3, it is observed that the values of $\|e_{\mathcal{I}}(\flat)\|$ approach zero before the fixed time τ_{max}. As depicted in Figure 4, the values of $k_{\mathcal{I}}^m(\flat)$ converge to positive bounded values. Consequently, the network (24) achieves fixed-time synchronization according to Theorem 3.1 and controller (8).

Figure 3. Evolution of $\|e_{\mathcal{I}}(\flat)\|, \mathcal{I} = 1,2,\cdots,5$ for system (24) via controller (8) with settling time $\tau_{max} = 3.54671\,\text{s}$.
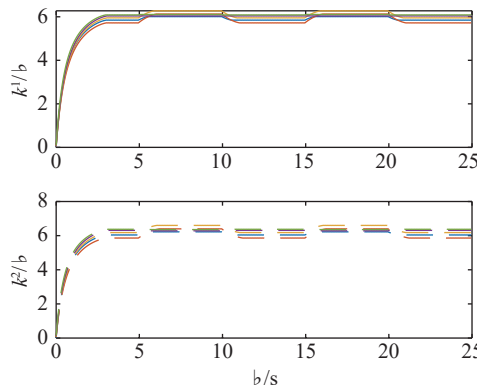
Figure 4. Evolution of adaptive gains $k_{\mathcal{I}}^m(\flat), m = 1,2$ of controller (8).

Example 4.3. To demonstrate the superiority of this paper's control strategy, we compare our adaptive fixed-time control (AFTC) approach with the node-based adaptive control (NBAC) strategy [42] and the adaptive proportional-integral control (APIC) method [11]. For fair comparisons, we use the same parameters as in Example 4.2.

The simulation results are shown in Figures 5 and 6. In Figure 5, AFTC exhibits a faster convergence speed compared to NBAC and APIC. As depicted in Figure 6, the adaptive gains of APIC are the lowest among the methods. However, APIC cannot ensure that the system error remains at lower values. Therefore, our control method demonstrates superior performance.
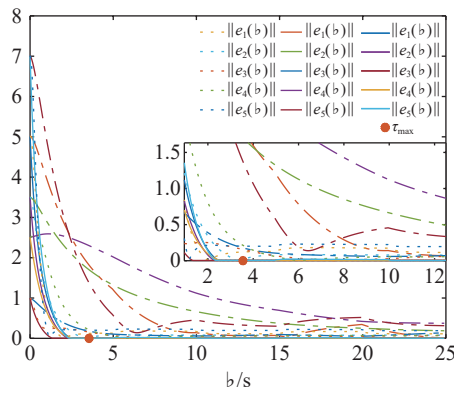
Figure 5. Evolution of $\|e_\jmath(\flat)\|, \jmath = 1, 2, \cdots, 5$ based on AFTC, NBAC, and APIC.
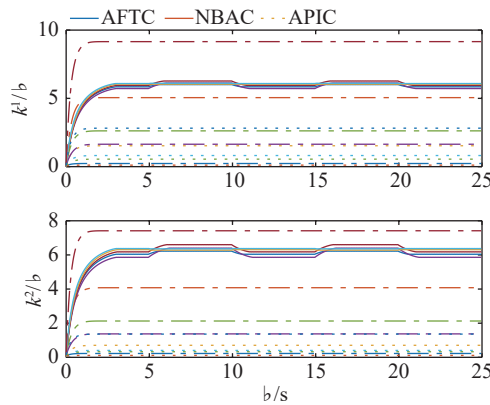
Figure 6. Evolution of adaptive gains $k_\jmath^m(\flat), m = 1, 2$ of AFTC, NBAC, and APIC.

5. Conclusion

In this paper, we have tackled the issue of fixed-time synchronization for a class of CNNs with multiple switching topologies. We derived a theoretical criterion to guarantee fixed-time synchronization and developed an adaptive fixed-time control strategy. To validate our findings, we presented two numerical examples demonstrating the correctness and effectiveness of the proposed approach.

Author Contributions: Linhao Zhao: formal analysis, funding acquisition, methodology, writing - original draft. **Boqian Li:** formal analysis, software, conceptualization, methodology.

Data Availability Statement: No data was used for the research described in the article.

Conflicts of Interest: The authors declare that they have no known competing financial interests or personal relationships that could have appeared to influence the work reported in this paper.

References

1. Zhou, J.; Chen, T.P.; Xiang, L. Chaotic lag synchronization of coupled delayed neural networks and its applications in secure communication. Circuits Syst. Signal Process, **2005**, *24*: 599−613. doi: 10.1007/s00034-005-2410-y

2. Ouyang, D.Q.; Shao, J.; Jiang, H.J.; *et al*. Impulsive synchronization of coupled delayed neural networks with actuator saturation and its application to image encryption. Neural Netw, **2020**, *128*: 158−171. doi: 10.1016/J.NEUNET.2020.05.016

3. Qiu, H.L.; Cao, J.D.; Liu, H. Passivity of fractional-order coupled neural networks with interval uncertainties. Math. Comput. Simul, **2023**, *205*: 845−860. doi: 10.1016/J.MATCOM.2022.10.029

4. Long, H.; Ci, J.X.; Guo, Z.Y.; *et al*. Synchronization of coupled switched neural networks subject to hybrid stochastic disturbances. Neural Netw, **2023**, *166*: 459−470. doi: 10.1016/J.NEUNET.2023.07.045

5. Tang, Z.; Jiang, C.H.; Wang, Y.; *et al*. Average impulsive weight based event-triggered impulsive synchronization on coupled neural networks. IEEE Trans. Netw. Sci. Eng, **2023**, *10*: 2180−2189. doi: 10.1109/TNSE.2023.3243248

6. Wang, J.L.; Zhang, X.X.; Wen, G.G.; *et al*. Passivity and finite-time passivity for multi-weighted fractional-order complex networks

with fixed and adaptive couplings. IEEE Trans. Neural Netw. Learn. Syst, **2023**, *34*: 894−908. doi: 10.1109/TNNLS.2021.3103809

7. Zhao, L.H.; Wen, S.P.; Xu, M.; *et al*. PID control for output synchronization of multiple output coupled complex networks. IEEE Trans. Netw. Sci. Eng, **2022**, *9*: 1553−1566. doi: 10.1109/TNSE.2022.3147786

8. Zhao, L.H.; Wen, S.P.; Li, C.J.; *et al*. A recent survey on control for synchronization and passivity of complex networks. IEEE Trans. Netw. Sci. Eng., **2022**, *9*: 4235−4254. doi: 10.1109/TNSE.2022.3196786

9. Wang, J.L.; Zhao, L.H. PD and PI control for passivity and synchronization of coupled neural networks with multi-weights. IEEE Trans. Netw. Sci. Eng., **2021**, *8*: 790−802. doi: 10.1109/TNSE.2021.3052889

10. Wu, X.Q.; Wu, X.Q.; Wang, C.Y.; *et al*. Synchronization in multiplex networks. Phys. Rep., **2024**, *1060*: 1−54. doi: 10.1016/j.physrep.2024.01.005

11. Cao, Y.T.; Zhao, L.H.; Zhong, Q.S.; *et al*. Adaptive PI control for H_∞ synchronization of multiple delayed coupled neural networks. Neurocomputing, **2023**, *560*: 126855. doi: 10.1016/J.NEUCOM.2023.126855

12. Liu, X.L.; Wang, J.L.; Huang, T.W. Output synchronization for coupled neural networks with multiple delayed output couplings. IEEE Trans. Circuits Syst. II Express Briefs, **2022**, *69*: 4394−4398. doi: 10.1109/TCSII.2022.3182702

13. Wang, L.; Bian, Y.G.; Guo, Z.Y.; *et al*. Lag H_∞ synchronization in coupled reaction-diffusion neural networks with multiple state or derivative couplings. Neural Netw., **2022**, *156*: 179−192. doi: 10.1016/J.NEUNET.2022.09.030

14. Galicki, M. Finite-time control of robotic manipulators. Automatica, **2015**, *51*: 49−54. doi: 10.1016/J.AUTOMATICA.2014.10.089

15. Wang, L.; Bian, Y.G.; Cao, D.P.; *et al*. Hierarchical safe control of heterogeneous connected vehicle systems using adaptive fault-tolerant control. *IEEE Trans. Veh. Technol*. **2024**, in press. doi:10.1109/TVT.2024.3400971

16. Bhat, S.P.; Bernstein, D.S. Finite-time stability of continuous autonomous systems. SIAM J. Control Optim., **2000**, *38*: 751−766. doi: 10.1137/S0363012997321358

17. Rao, H.X.; Guo, Y.R.; Xu, Y.; *et al*. Nonfragile finite-time synchronization for coupled neural networks with impulsive approach. IEEE Trans. Neural Netw. Learn. Syst., **2020**, *31*: 4980−4989. doi: 10.1109/TNNLS.2020.3001196

18. Tang, R.Q.; Su, H.S.; Zou, Y.; *et al*. Finite-time synchronization of Markovian coupled neural networks with delays via intermittent quantized control: Linear programming approach. IEEE Trans. Neural Netw. Learn. Syst., **2022**, *33*: 5268−5278. doi: 10.1109/TNNLS.2021.3069926

19. Xu, Y.H.; Gao, Q.W.; Xie, C.R.; *et al*. Finite-time synchronization of complex networks with privacy-preserving. IEEE Trans. Circuits Syst. II Express Briefs, **2023**, *70*: 4103−4107. doi: 10.1109/TCSII.2023.3274634

20. Tian, E.G.; Zou, Y.; Chen, H.T. Finite-time synchronization of complex networks with intermittent couplings and neutral-type delays. IEEE/CAA J. Autom. Sin., **2023**, *10*: 2026−2028. doi: 10.1109/JAS.2023.123171

21. Qiu, S.H.; Huang, Y.L.; Ren, S.Y. Finite-time synchronization of multi-weighted complex dynamical networks with and without coupling delay. Neurocomputing, **2018**, *275*: 1250−1260. doi: 10.1016/J.NEUCOM.2017.09.073

22. Xu, Y.; Li, Y.Z.; Li, W.X. Adaptive finite-time synchronization control for fractional-order complex-valued dynamical networks with multiple weights. Commun. Nonlinear Sci. Numer. Simul., **2020**, *85*: 105239. doi: 10.1016/J.CNSNS.2020.105239

23. Zhao, L.H.; Wen, S.P.; Guo, Z.Y.; *et al*. Finite-time nonchattering synchronization of coupled neural networks with multi-weights. IEEE Trans. Netw. Sci. Eng., **2023**, *10*: 2212−2225. doi: 10.1109/TNSE.2023.3243610

24. Wang, J.L.; Wu, H.Y.; Huang, T.W.; *et al*. Finite-time synchronization and H∞ synchronization for coupled neural networks with multistate or multiderivative couplings. IEEE Trans. Neural Netw. Learn. Syst., **2024**, *35*: 1628−1638. doi: 10.1109/TNNLS.2022.3184487

25. Polyakov, A. Nonlinear feedback design for fixed-time stabilization of linear control systems. IEEE Trans. Autom. Control, **2012**, *57*: 2106−2110. doi: 10.1109/TAC.2011.2179869

26. Chen, X.Y.; Jia, T.Y.; Wang, Z.S.; *et al*. Practical fixed-time bipartite synchronization of uncertain coupled neural networks subject to deception attacks via dual-channel event-triggered control. IEEE Trans. Cybern, **2024**, *54*: 3615−3625. doi: 10.1109/TCYB.2023.3338165

27. Gong, S.Q.; Guo, Z.Y.; Wen, S.P.; *et al*. Finite-time and fixed-time synchronization of coupled memristive neural networks with time delay. IEEE Trans. Cybern, **2021**, *51*: 2944−2955. doi: 10.1109/TCYB.2019.2953236

28. Guo, Z.Y.; Xie, H.; Wang, J. Finite-time and fixed-time synchronization of coupled switched neural networks subject to stochastic disturbances. IEEE Trans. Syst. Man Cybern. Syst, **2022**, *52*: 6511−6523. doi: 10.1109/TSMC.2022.3146892

29. Cao, Y.T.; Zhao, L.H.; Zhong, Q.S.; *et al*. Adaptive fixed-time output synchronization for complex dynamical networks with multi-weights. Neural Netw, **2023**, *163*: 28−39. doi: 10.1016/J.NEUNET.2023.03.032

30. Liu, X.Y.; Shao, S.; Hu, Y.F.; *et al*. Fixed-time synchronization of multi-weighted complex networks via economical controllers. Neural Process. Lett, **2022**, *54*: 5023−5041. doi: 10.1007/S11063-022-10846-1

31. Shi, J.Y.; Zhou, P.P.; Cai, S.M.; *et al*. On finite-/fixed-time synchronization of multi-weighted dynamical networks: A new unified control approach. Neural Comput. Appl, **2023**, *35*: 5769−5790. doi: 10.1007/S00521-022-07979-8

32. Wen, G.H.; Yu, X.H.; Yu, W.W.; *et al*. Coordination and control of complex network systems with switching topologies: A survey. IEEE Trans. Syst. Man Cybern. Syst, **2021**, *51*: 6342−6357. doi: 10.1109/TSMC.2019.2961753

33. Hu, T.T.; Park, J.H.; Liu, X.Z.; *et al*. Sampled-data-based event-triggered synchronization strategy for fractional and impulsive complex networks with switching topologies and time-varying delay. IEEE Trans. Syst. Man Cybern. Syst, **2022**, *52*: 3568−3580. doi: 10.1109/TSMC.2021.3071811

34. Yang, Q.J.; Wu, H.Q.; Cao, J.D. Pinning exponential cluster synchronization for fractional-order complex dynamical networks with switching topology and mode-dependent impulses. Neurocomputing, **2021**, *428*: 182−194. doi: 10.1016/J.NEUCOM.2020.11.031

35. Chen, Y.G.; Wang, Z.D.; Hu, J.; *et al*. Synchronization control for discrete-time-delayed dynamical networks with switching topology under actuator saturations. IEEE Trans. Neural Netw. Learn. Syst, **2021**, *32*: 2040−2053. doi: 10.1109/TNNLS.2020.2996094

36. Yang, X.S.; Li, X.D.; Lu, J.Q.; *et al*. Synchronization of time-delayed complex networks with switching topology via hybrid actuator fault and impulsive effects control. IEEE Trans. Cybern, **2020**, *50*: 4043−4052. doi: 10.1109/TCYB.2019.2938217

37. Wang, S.B.; Cao, Y.T.; Guo, Z.Y.; *et al*. Periodic event-triggered synchronization of multiple memristive neural networks with switching topologies and parameter mismatch. IEEE Trans. Cybern, **2021**, *51*: 427−437. doi: 10.1109/TCYB.2020.2983481

38. Wang, J.L.; Wang, L.; Wu, H.N. Synchronization for complex networks with multiple state or delayed state couplings under recoverable attacks. IEEE Trans. Syst. Man Cybern. Syst, **2023**, *53*: 38−48. doi: 10.1109/TSMC.2022.3164792

39. Cao, Y.T.; Zhao, L.H.; Zhong, Q.S.; *et al*. Synchronization of coupled neural networks with multiple switching topologies via adaptive control techniques. Int. J. Robust Nonlinear Control, **2024**, *34*: 8661−8675. doi: 10.1002/rnc.7409

40. Hardy, G.H.; Littlewood, J.E.; Pólya, G. *Inequalities*, 2nd ed.; Cambridge University Press: Cambridge, 1952.
41. Horn, R.A.; Johnson, C.R. *Topics in Matrix Analysis*; Cambridge University Press: Cambridge, 1991.
42. Zhao, L.H.; Wen, S.P.; Zhu, S.; *et al*. Robust H_∞ pinning synchronization for multiweighted coupled reaction-diffusion neural networks. IEEE Trans. Cybern, **2023**, *53*: 6549−6561. doi: 10.1109/TCYB.2022.3223713